Tidal Turbine Benchmarking Project: Stage I - Steady Flow Blind Predictions

R H J Willden, Xiaosheng Chen, S W Tucker Harvey, H Edwards, C R Vogel, K Bhavsar, T Allsop, J Gilbert, H Mullings, M Ghobrial, et al.

Tidal Turbine Benchmarking Project: Stage I - Steady Flow Blind Predictions

R.H.J. Willden[1*], X. Chen[1], S.W. Tucker Harvey[1], H. Edwards[1], C.R. Vogel[1], K. Bhavsar[2], T. Allsop[2], J. Gilbert[2], H. Mullings[3], M. Ghobrial[3], P. Ouro[3], D. Apsley[3], T. Stallard[3], I. Benson[4], A. Young[4], P. Schmitt[5], F. Zilic de Arcos[6], M.-A. Dufour[6], C. Choma Bex[6], G. Pinon[6], A.I. Evans[7], M. Togneri[7], I. Masters[7], L.H. da Silva Ignacio[8], C.A.R. Duarte[8], F.J. Souza[8], S. Gambuzza[9], Y. Liu[9], I.M. Viola[9], M. Rentschler[10], T. Gomes[10], G. Vaz[10], R. Azcueta[11], H. Ward[11], F. Salvatore[12], Z. Sarichloo[12], D. Calcagni[12], T.T. Tran[13], H. Ross[13], M. Oliveira[14], R. Puraca[14] & B.S. Carmo[14]

***Abstract*—This paper presents the first blind prediction stage of the Tidal Turbine Benchmarking Project conducted and funded by the UK's EPSRC and Supergen ORE Hub. In this first stage, only steady flow conditions, at low and elevated turbulence levels (3.1%), were considered. Prior to the blind prediction stage, a large laboratory-scale experiment was conducted in which a highly instrumented 1.6 m diameter tidal rotor was towed through a large towing tank in well-defined flow conditions with and without an upstream turbulence grid.**

Details of the test campaign and rotor design were released as part of this community blind prediction exercise. Participants were invited to simulate turbine performance and loads using appropriate methods. 26 submissions were received from 12 groups across academia and industry using techniques ranging from blade resolved Computational Fluid Dynamics through Actuator Line, Boundary Integral Equation Model, Vortex methods to engineering Blade Element Momentum methods.

The comparisons between experiments and blind predictions were very positive, not only helping to provide validation and uncertainty estimates for the models, but also validating the experimental tests themselves. The exercise demonstrated that the experimental turbine data provides a robust dataset against which researchers and engineers can test their models and implementations, helping to reduce uncertainty and provide increased confidence in engineering processes, as well as a basis against which modellers can evaluate and refine approaches.

***Index Terms*—Tidal turbine, blind prediction, benchmarking.**

I. Introduction

UNCERTAINTY in the loading of tidal stream turbines can contribute significantly to conservatism in turbine design. This uncertainty originates not only from limited knowledge of the flow-field at a particular site, but also from uncertainty in modelling fidelity together with unresolved questions relating to the fundamental physics which governs the loading and performance of tidal turbines in unsteady and turbulent flow regimes. To reduce this conservatism the engineering models used in turbine design must be improved. Validation of these models requires experimental data. However, few well-documented experimental data sets are available for tidal turbines, especially at scales large enough to provide multiple measurements along the blade span and achieve Reynolds number independence in order to facilitate comparison to full-scale devices.

There exist a number of experimental studies on tidal turbine performances, ranging from simple cases such as a single turbine in uniform flow conditions [1]–[3], to more complex conditions, with inflow turbulence [4], waves and shear [5], and multiple turbines interacting [6]. Yet few of these studies have led to the generation of well-documented data sets that could be utilised for model validation, especially at scales large enough to obtain Reynolds number independence and hence comparability to full-scale devices and with more detailed measurements like bending moments and moment/force distributions along the blade span.

The Tidal Turbine Benchmarking Project [7], funded by the UK's EPSRC and the Supergen ORE Hub, has conducted a large laboratory-scale experiment on a highly instrumented 1.6 m diameter tidal rotor in well-defined flow conditions, defined in [8]. In brief, the turbine, which is instrumented for torque, thrust as well as root and in-blade flapwise and edgewise bending moments at various spanwise positions, is towed through a large still water towing tank at QinetiQ's Haslar facility. Using a towing tank has the effect of presenting a low blockage level, which is desirable, but also a very low turbulence level, which is undesirable, and so a large turbulence grid was constructed and towed upstream of the test turbine to generate a homogenized elevated turbulent flow condition at the rotor. The experiments present a well-defined and highly repeatable set of test conditions, which are important facets when developing a validation data set. The flow blockage is low (3.05%), the blade Reynolds numbers post-critical, and the stream turbulence elevated to modest levels (3.1%), rendering the benchmark experiment results useful for validation of engineering and research models intended for use in the design and analysis of commercial-scale devices. Further details of the test campaign specification and rotor design [8] were released as part of this community blind prediction exercise, in which participants were invited to use a range of modelling approaches to simulate the performance and loads experienced by the turbine.

The benchmarking programme is divided into 2 stages. In this first stage (I) the turbine is tested and simulations

* Corresponding author: richard.willden@eng.ox.ac.uk

[1] Dept. Engineering Science, University of Oxford, UK. [2] Faculty of Science and Engineering, University of Hull, UK. [3] Dept. Mechanical, Aerospace and Civil Engineering, University of Manchester, UK. [4] Dept. Mechanical Engineering, University of Bath, UK. [5] Sch. Natural and Built Environment, Queen's University Belfast, UK. [6] LOMC, UMR CNRS 6294 Université Le Havre Normandie, France. [7] Mechanical Engineering, University of Swansea, UK. [8] Federal University of Uberlândia, Brazil. [9] Sch. of Engineering, University of Edinburgh, UK. [10] blueOasis R&D, Ericeira, Portugal. [11] Cape Horn Engineering Ltd., Portsmouth, UK. [12] CNR-INM, Roma, Italy. [13] NREL, Golden, CO, USA. [14] Dept. Mechanical Engineering, University of São Paulo, Brazil.

Digital Object Identifier: https://doi.org/10.36688/ewtec-2023-574

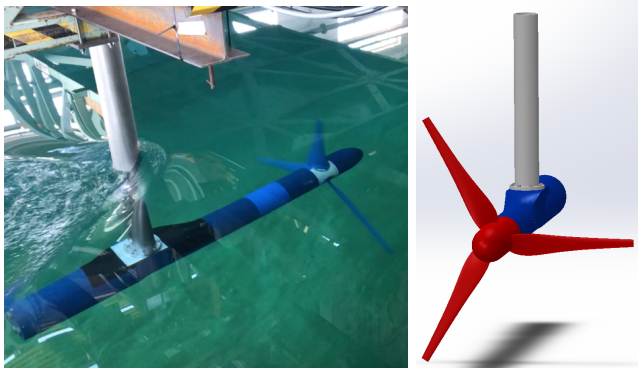

(a) Turbine being towed. (b) Turbine CAD.

Fig. 1: Design and testing of the benchmarking turbine.

benchmarked under steady flow conditions with low and grid generated elevated inflow turbulence. A second stage (II) of experiments and benchmarking exercise is ongoing in which the turbine is being tested under current and incident head wave conditions. This paper presents the results of the stage I benchmarking exercise and analysis of the submitted data, whilst details of the design, testing and experimental results are presented in a companion paper [8].

Section II provides a brief description of the model setup, with details of the participating groups and the modelling approaches employed. The analysis of the results of the benchmarking exercise are provided in section III in two parts: integrated rotor quantities (thrust and power), followed by spanwise force and moment distributions. In both parts, the data are analysed and presented in a number of different ways and by modelling method to help develop further insights into the features and applicability of each simulation technique, as well as their similarities and deviations.

An important aspect of this benchmarking exercise is to develop confidence in modelling techniques, their correct application, where different models can and can't be used and the relative trade-offs of cost, complexity and accuracy. Understanding and quantifying the errors and uncertainties in different modelling technique being just as important as refining their accuracy.

II. Experiments, test and condition specifications

A brief introduction to the Stage I steady experiments is first given here. A tidal turbine with rotor diameter D of 1.6 m was tested in the Haslar towing tank facility. At a tow speed of 1.0 m/s the facility allows 2-3 minutes of steady tow, and with a width of 12.2 m and depth of 5.4 m, provides a low global blockage of 3.05% (ratio of turbine-to-channel cross-sectional areas). The turbine was towed with a 0.22 D tip-to-surface clearance. For all experiments a settling time of 15 minutes was used between tests, and each test case was conducted three times to ensure repeatability and robustness of results. Two sets of data were collected and used for the benchmarking exercise; *Low Turbulence* (LT) cases run in still water (turbulence intensity, Tu $\approx$ 0), and *Elevated Turbulence* (ET) cases run with an upstream towed turbulence grid. The grid was pushed 5.0 m ahead of the turbine and generated a homogenized flow at the rotor plane with Tu = 3.1% and flow speed of 0.899 m/s (with the turbine and grid towed at 1.0 m/s). An image of the rotor being towed together with the rotor-nacelle-tower CAD model is shown in Fig. 1.

The turbine was tested at a single tow speed of 1.0 m/s. A range of tip-speed ratios, λ, were achieved by altering the turbine's rotational speed, ω, with,

$$\lambda = R\omega/U_\infty\,, \tag{1}$$

where R is the rotor radius and U_∞ is the flow speed at the rotor plane in the absence of the turbine. Based on the available measurement database, the cases used for the benchmark exercise were determined and are listed in Table I. The table highlights the priority cases which all participants were asked to concentrate on as well as further optional cases. Note that the analysis of the experimental flow data for the elevated turbulence case evolved with the use of both Acoustic Doppler Velocimetry (ADV) and dynamic pressure based measurements, with the latter eventually proving more accurate. Hence, it was determined after the benchmarking exercise had been initiated that the experimental tip-speed ratios (TSRs) were slightly different from those run by contributing modellers. As all data are plotted non-dimensionally, this discrepancy does not introduce any error save for the assumption of Reynolds number independence over the few percentage change in flow speed. Where necessary to make quantitative comparison at given TSRs, the experimental data, which varied smoothly with TSR, have been interpolated to the tip-speed ratio values used by modellers.

So that the exercise could concentrate on identifying and understanding differences between modelling approaches, every attempt was made to eliminate common modelling data discrepancies and interpretation issues; the flow conditions were well defined, experiments repeated, and the blade uses a constant hydrofoil section, including constant trailing edge thickness-to-chord ratio, along the entire blade span. Differences in modelling outputs can often originate from differences in hydrodynamic input data (lift and drag coefficients) used by models, and so lift and drag input data, see Fig. 2, were simulated and provided to the modellers who were free to use either this or alternative data as they wished. Additional data was provided for the benchmarking exercise [7], including the rotor and facility geometries, further test conditions, blade profiles and foil performance data.

III. The benchmarking exercise

The Stage I benchmarking exercise received 26 submissions from 12 research groups from across the world. Most of the submissions can be categorised into 3 major methodologies: Blade Element Momentum (BEM) based methods, Computational Fluid Dynamics (CFD) blade resolved (BR) methods, and Actuator Line (AL) methods that are embedded within CFD simulations. Additional submissions were received from contributors using the Boundary Integral Equation Model (BIEM) and Vortex based methods. A summary of all the submissions and their contributors is provided in Tables II to IV. The methodologies are briefly introduced below.

A. Blade Element Momentum methods

BEM combines blade element and momentum theories to provide a quick and tractable tool for modelling turbine performance and loads. It was first introduced by Froude in 1878 to model airscrews, with later refinements by Glauert (1920) and Betz (1921). The method assumes that individual spanwise sections of a rotor blade can be treated independently

TABLE I: Benchmark simulation cases, with priority cases highlighted in yellow.

Low Turbulence (LT) Cases													
Case No.	I	II	III	IV	V	VI	VII	VIII	IX	X	XI	XII	XIII
U_∞ [m/s]	1.0	1.0	1.0	1.0	1.0	1.0	1.0	1.0	1.0	1.0	1.0	1.0	1.0
λ	4.02	4.52	5.03	5.36	5.53	5.78	6.03	6.53	6.70	7.04	7.20	7.54	7.87

Elevated Turbulence (ET) Cases											
Case No.	I	II	III	IV	V	VI	VII	VIII	IX	X	XI
U_∞ [m/s]	0.9207	0.9207	0.9207	0.9207	0.9207	0.9207	0.9207	0.9207	0.9207	0.9207	0.9207
λ	3.91	4.46	4.91	5.37	5.64	5.82	6.19	6.37	6.92	7.37	7.73

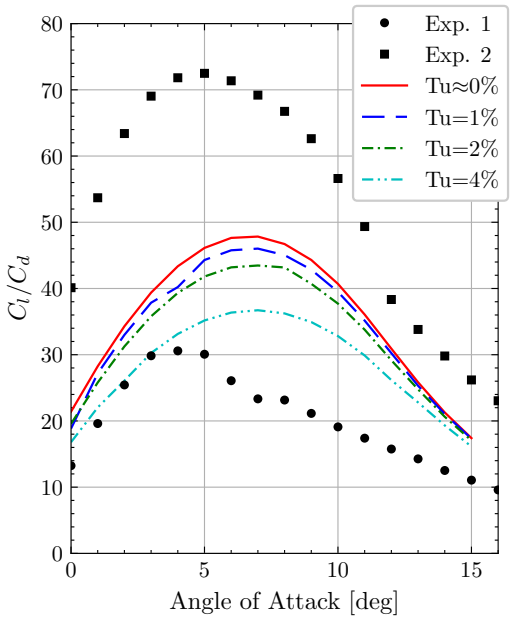

Fig. 2: Hydrofoil lift-to-drag ratios at turbulence intensity (Tu) levels from 0.1% to 4% simulated using 2D RANS with $k-\omega$ SST turbulence closure ($\mathrm{Re} = 2.88 \times 10^5$), and comparisons to experimental data; Exp. 1 at $\mathrm{Re} = 3.2 \times 10^5$ [9] and Exp. 2 at $\mathrm{Re} = 1.6 \times 10^6$ [10].

and that the foil behaves locally two-dimensionally and can be modelled through sectional data. The hydrodynamic forces, lift, l, and drag, d, are calculated on each individual blade section of span length δr. The blade section is swept azimuthally to form an annular blade ring. The blade element rings together form the rotor disk. Each of the rings is related to an annular streamtube which captures the flow passing through that ring. It is assumed that the streamtubes are independent of each other and radial flows between rings are neglected. A number of different BEM models are adopted by the participating modellers, with a variety of different data inputs and correction models, including various 2D hydrofoil polars, turbulence representations, high-induction corrections etc. Table II summarises the key parameters of the participant BEM methods, with further details provided below.

LOMC-BEM submission is contributed by the LOMC research group from the Université Le Havre Normandie, who utilised a BEM solver with method originating from [11] with iterative convergence based on inflow angle ϕ instead of on axial and tangential induction factors a and a'. The 2D lift and drag coefficient polars were calculated from a set of 2D wall-resolved Reynolds-averaged Navier-Stokes (RANS) simulations of the hydrofoil at various local-chord-based Re and Tu using the k-ω SST closure. The polar data are interpolated along the blade span based on local Re and

TABLE II: Summary of BEM submissions and models used.

Submission	2D Polars	Induction/Wake Correction	Hub/Tip Models
LOMC-BEM	2D RANS	Modified turbulent wake model	None/PDL †
NREL-BEM	Provided* with rotation correction	Buhl model	PDL
SU-BEM	Provided	High-induction model	PDL
UoE-BEM	XFOIL	Buhl model	GLT ‡
UFU-BEM-Aerodas	Provided with Aerodas correction	None	PDL
UFU-BEM-SD	Provided with stall delay correction	None	PDL
UoM-BEM-1	Provided	Glauert	None/GLT
UoM-BEM-2	Provided	Glauert	GLT

* 2D performance polars provided as part of the benchmarking exercise (from 2D RANS). † PDL = Prandtl-type hub / tip correction. ‡ GLT = Glauert-type hub / tip correction.

Tu values. The BEM solver utilises a modified turbulent wake model [12] which increases the turbine thrust at high induction factors above that of more traditional Buhl models.

NREL-BEM submission contributed by the National Renewable Energy Laboratory (NREL) was completed using an in-house solver AeroDyn [13], a module of the whole turbine simulation code OpenFAST. AeroDyn uses the iterative solution procedure proposed by Ning [11]. Tower effects were neglected, a steady uniform inflow was assumed, loads on the hub and nacelle were omitted, and no additional features for marine turbines (buoyancy, added mass loads etc.) were considered. Glauert's empirical correction with Buhl's modification was used for high induction correction. Optional empirical corrections were used including the Pitt and Peters skewed wake model, the Prandtl hub/tip loss corrections, unsteady aerodynamics (Minnema/Pierce variation of the Beddoes-Leishman model), and tangential induction (drag term included). The provided sectional foil data was corrected by an in-house code for 3D rotational effects.

SU-BEM submission used the method developed by Swansea University [14]. Each blade was represented by 176 radial elements of equal length 0.004 m. Prandtl tip and hub loss models and high-induction correction factors were used. The 2D hydrofoil data used were as provided for Tu = 0.01% only, with no interpolation along the blade span. Turbulence is accounted for using the Sandia method to produce 3D flow fields that are non-physical but match statistical properties of real flow at low computational expense [15].

UoE-BEM submission used the University of Edinburgh's in-house BEM code, transTide, originally developed in [16], with subsequent developments to allow changes in the blade hydrodynamic properties along the blade span. The BEM

model includes a synthetic turbulence generator and the ability to model the hydrodynamics of surface waves (not used for the current simulations). The 2D hydrofoil data used were generated from external XFOIL simulations [17] with significant attention paid to resulting BEM results uncertainty originating from stochastic variations in foil lift and drag data.

UFU-BEM-Aerodas and *UFU-BEM-SD* submissions from the Federal University of Uberlandia (UFU) use the BEM code QBlade developed by the Technique University of Berlin [18]. The provided 2D polars were corrected by the Aerodas [19] and Stall Delay (SD) [20] models. Linear interpolation of the polar data between Tu = 2% and 4% was used to develop input data for the elevated turbulence case at Tu = 3.1%.

UoM-BEM-1 submission from the University of Manchester used an in-house Fortran-based BEM code which is a further development on that documented in [21]. This includes a Prandtl-Glauert tip correction and Glauert high-axial-induction correction. The code can accommodate time-dependent inflow, yaw and a vertical velocity profile, but has no corrections at present for nacelle, supports, blockage, turbulent intensity or Reynolds number dependence. The provided polars at different Tu levels were used, following confirmatory simulations using an in-house RANS code of the accuracy of the provided 2D polars.

UoM-BEM-2 submission used a different in-house BEM code [22], with a resolution of 176 elements along each blade, with a single provided lift/drag polar at the lowest Tu level being used. Tip and hub losses are accounted for through Prandtl's tip loss and Glauert's correction for highly loaded rotors where needed, and an induction model is applied using the Glauert high-axial-induction correction. Further model features include a synthetic turbulent flow field model [23], a tower shadow model and a model for the influence of high-frequency fluctuations from blade-generated flow [22].

B. Actuator Line methods

The AL method is an unsteady method in which each blade is represented virtually as it rotates through a domain in which the governing flow equations are advanced using a CFD solver. The method was originally proposed for studying wind turbine wake dynamics by [24]. By using a discrete blade representation, the AL method is able to capture discrete blade effects such as tip vortices and the rotor's helical wake, which is not possible using azimuthally-averaged actuator disc type methods such as BEM. In the AL method the blades are replaced by equivalent point forces that are computed at collocation points that are distributed along the span of each blade, usually along the locus of the blade's centre of pressure and clustered in the spanwise direction around the blade root and tip. In each time step the flow-field is sampled at or around each of the collocation points and foil lift and drag data are used to compute the resulting blade loads that are then imposed on the flow-field so that the simulation can be advanced in time. The virtual blades are rotated through a static computational domain to simulate the rotation of the rotor, without resolving the physical geometry of the blades, thus offering substantial cost savings relative to blade resolved methods. Flow blockage and boundary proximity are implicitly modelled through the specification of the simulation domain. Table III summarises the key parameters of the participating AL methods.

QUB-AL-LES submission from Queen's University Belfast used a developmental AL code [25] which was forked from the original implementation in [26] based on OpenFOAM Large-eddy Simulation (LES) solver. The simulation is carried out using 44 collocation points per blade on a 16.3M cell mesh, with nacelle and tower not simulated. The provided 2D hydrofoil data at Tu $\approx$ 0% and 4% are used for the LT and ET cases. A Shen et al. [27] model is used to provide outboard blade load relief to account for three-dimensional flow effects.

TABLE III: Summary of AL submissions and models used.

Submission	Turbulence Model	2D Polars	Nacelle Model	Tip-loss Model
QUB-AL-LES	OpenFOAM LES Smagorinsky	Provided*	None	SM ‡
UoM-AL-uRANS	STREAM k-ω SST	Provided	IB †	None
UoM-AL-LES	DOFAS LES WALE	Provided	IB	SM
UoO-AL-NRSM	OpenFOAM k-ω SST	Provided	Resolved	SM
UoO-AL-NRWM	OpenFOAM k-ω SST	Provided	Resolved	WM ‡
UoO-AL-IBWM	OpenFOAM k-ω SST	Provided	IB	WM

*2D performance polars provided as part of the benchmarking exercise (from 2D RANS). † IB = Immersed Boundary method. ‡ SM & WM = Shen et al.- and Wimshurst & Willden-type tip-loss models.

UoM-AL-uRANS from the University of Manchester used an in-house code, STREAM [21], with k-ω SST turbulence model, 3rd-order advection (UMIST) and 2nd-order time-stepping (Crank-Nicolson) schemes. Uniform inflow was prescribed, with turbulence intensity to match each experiment and a low dissipation rate to ensure propagation of conditions to the turbine. Side walls and top/bottom surfaces were approximated by symmetry planes to avoid resolving boundary layers. The provided foil coefficients for Tu $\approx$ 0 were used throughout. The nacelle was modelled using an Immersed Boundary (IB) method to avoiding costly boundary meshing.

UoM-AL-LES used another in-house code DOFAS [23], [28] with turbulence modelled through a LES approach with the WALE sub-grid scale model. A 30M cell mesh with $0.025D$ grid resolution in all directions was used. The free surface is modelled as non-deforming, the nacelle modelled using an IB method, and the Shen et al. load correction applied to the rotor forces.

UoO-AL-NRSM / NRWM / IBWM submissions from the University of Oxford use OpenFOAM to solve the RANS equations with the k-ω SST model and 2nd-order spatial and temporal discretisation. Two meshes are used: a nacelle-resolving (NR) mesh for the NRSM / NRWM cases, and a mesh with similar resolution and an IB nacelle representation (IBWM case). The AL model was initially developed in [29], further modified by [30], has multi-parameter lift-drag polar interpolation methods, uses a line-averaging velocity sampling technique [31] and has two tip-loss correction models available: the Shen et al. [27] model which applies the same correction to axial and tangential forces (NRSM case) and the Wimshurst & Willden [30] model that is a recalibration of [27] to provide greater load relief in the torque direction through an anisotropic correction (IBWM / NRWM cases).

C. Blade Resolved methods

Blade Resolved simulations are the most computationally intensive of all of the solution methods, but also the simplest

TABLE IV: Summary of BR submissions and models used.

Submission	Turbulence Model	State	Flow Domain
blueOASIS-BR-RANS	ReFRESCO 2.8.0 k-ω SST	Steady	MRF* WR§
CHE-BR-uRANS	STAR-CCM+ k-ω SST	Unteady	TTG † VOF ‡
CNR-INM-BR-uRANS	X NAVIS SA	Unsteady	MRF WR
LOMC-BR-RANS	OpenFOAM k-ω SST	Steady	MRF
NREL-BR-RANS	STAR-CCM+ k-ω SST	Steady	MRF
NREL-BR-uRANS	STAR-CCM+ k-ω SST	Unsteady	TTG VOF
UoE-BR-RANS	OpenFOAM k-ω SST	Steady	MRF
UoO-BR-RANS	OpenFOAM k-ω SST	Steady	MRF
USP-BR-DES	OpenFOAM DES SST	Unsteady	TTG

* MRF = multiple reference frame technique with by default a 120° cylindrical wedge domain of a single blade, or if specified the § WR = whole rotor geometry. † TTG = tow-tank geometry with rotating turbine submerged at experimental depth. ‡ VOF = Volume-of-Fluid free surface representation.

conceptually with no specific requirement for empirical data inputs. The CFD solver simulates the flow through the fluid domain with the blade surface and turbine nacelle modelled as boundaries. Table IV presents the major features and differences between the participant-submitted BR solutions. Aside from mesh resolution, the significant differences between the methods are turbulence closure, whether the simulations are steady or unsteady, whether a Multiple Reference Frame (MRF) approach is followed, often with a single blade in a 120° wedge domain (with one exception simulating the whole rotor, WR) to simulate the flow relative to the blade / rotor, or if the whole rotating rotor is simulated in a domain matching the tow-tank geometry (TTG), and then whether the free surface is represented as un-deforming or by using a Volume-of-Fluid (VOF) free surface capturing approach.

blueOASIS-BR-RANS from industry consultancy blueOASIS uses a community-based, open-usage, viscous-flow CFD code ReFRESCO [32], that has been used in previous tidal turbine studies [33]. The solver is incompressible, and the SIMPLE algorithm and the k-ω SST transitional model were used. An unstructured mesh was generated using commercial software Hexpress, with 34.3M cells and a fully resolved blade surface (first cell height $y^+ < 1$). A steady MRF approach was followed to simulate the whole rotor.

CHE-BR-uRANS from industry consultancy Cape Horn Engineering, used STAR-CCM+ to perform unsteady RANS with the k-ω SST turbulence model and VOF approaches. A VOF adaptive mesh refinement (AMR) model was used to reduce unnecessary cell count. The full turbine, rotor, nacelle, and tower, as well as the tank walls and floor were modelled.

CNR-INM-BR-uRANS submission from CNR-INM utilised an in-house unsteady incompressible RANS solver with the Spalart-Allmaras turbulence model [34]. The simulations used the MRF technique but with all 3 blades simulated. A three-level multi-grid approach was adopted to speed-up the convergence of the solution, with the finest mesh requiring about 1.5M cells per blade using an overlapping o-grid technique and a wall-resolving mesh ($y^+ < 10$).

LOMC-BR-RANS from LOMC performed incompressible RANS simulations in OpenFOAM with the k-ω SST model. A one-third cylindrical domain MRF approach was used with a 26M cell wall-resolving mesh.

NREL-BR-RANS / uRANS are contributed by NREL, using the commercial CFD code STAR-CCM+. The steady solutions are of a single blade and one-third hub using the MRF approach, and 4 different grid resolutions were used to quantify spatial discretisation uncertainty for the low turbulence case. For the unsteady simulations the whole turbine geometry, rotor, nacelle and tower, were resolved, with the rotor simulated inside a rotating mesh with sliding interface to the static outer domain, submerged to the correct depth with VOF used to model surface deformation, hydrostatic and buoyancy effects.

UoE-BR-RANS from the University of Edinburgh used OpenFOAM with steady RANS and the k-ω SST model. A one-third rotor MRF technique was used with a non-conformal structured 19M hexahedral cell mesh. The blade's boundary layer was resolved with an average y^+ of 0.35 at $\lambda = 6$.

UoO-BR-RANS simulations by the University of Oxford used a one-third domain steady MRF approach in OpenFOAM with k-ω SST turbulence closure. A 38M cell mesh was carefully generated with fully hexahedral cells and a resolved boundary layer with first wall cell height $y^+ < 1$.

USP-BR-DES from the University of São Paulo, used an unsteady approach with a hybrid Detached Eddy Simulation (DES) and k-ω SST turbulence model [35]. The rotating sliding meshing strategy followed [36] and data exchange between fixed and rotating meshes used an Arbitrary Mesh Interface (AMI) technique. Wall functions were used with the first cell height varying $y^+ \approx 30 \rightarrow 100$ at $\lambda = 6.03$.

D. Other approaches

Solutions using other methods were received as follows.

CNR-INM-BIEM-D12 / D22 were received from CNR-INM and use the Boundary Integral Equation Model. The method solves Laplace's equation for the velocity potential of the flow over the rotor in an integral formulation [37]. A simple Viscous Flow Correction (VFC) model has been developed to estimate the effects of viscosity on blade loads. In the present study, the VFC model has been applied with input 2D flow lift and drag curves calculated using XFOIL [17] over relevant ranges of angle-of-attack and Reynolds number. The suffix D12 / D22 refers to alternative shape parameters used in modelling the curvature of the wake surface in the tip vortex region.

LOMC-Vortex contributed by LOMC employs a 3D unsteady Lagrangian Vortex Particle Method code, Dorothy, which represents the flow as a system of vorticity carrying particles [38]. The code can account for turbulent inflow and multi-wake interaction [39]. A lifting line model represents the blades, with tabulated lift and drag coefficients, together with blade-induced velocities from the previous time-step.

IV. Results Analysis

Following distribution and discussion of the test conditions and turbine geometry, the participating groups submitted their predictions of turbine power and thrust, as well as spanwise loading and bending moment distributions for the range of evaluation cases. Most submissions were received for the Low turbulence case (24) with somewhat fewer received for the Elevated turbulence case (17) with the reduction between the two being mostly driven by model and time restrictions not

permitting the explicit simulation of higher turbulence levels. Solutions for the priority TSR cases were received from all contributors able to simulate the given turbulence level, whilst some participants, particularly those with lower cost models, were able to submit the full set of cases in Table I.

We categorised the submitted data into 2 levels. The first level (L1) corresponds to the fully blind initial submissions, whilst the second level (L2) refers to submissions in which only user input errors or similar were corrected. Such user-corrected errors originated from, for example, misunderstanding of the turbine data or flow conditions, incorrect fluid properties etc, and whilst these are genuine modelling errors, they are not a reflection on the engineering models whose accuracy and validity this exercise is designed to test. We therefore concentrate on the presentation of L2 results. Comparisons between L1 and L2 are shown in Fig. 4 and Table V.

However, through the process of the benchmarking exercise it became apparent that the existence of a high-quality experimental data set, with test specifications and details having been examined, implemented and tested by more than a dozen groups, is a very valuable resource to enable modellers to sense-check their turbine modelling approaches. We therefore additionally report changes in solutions from L1 to L2 to highlight the value of the data set in reducing user type input errors that were hitherto undetected.

The benchmark data set has since been used by several groups to update and improve their physics and engineering models, which should result in further model improvements. We refer to such new solutions obtained post-release of the benchmark data as level L3. Such L3 results are not studied in this paper and are left for the participant groups to present.

The results presented and discussed below include integral quantities and bending moments. These are presented and discussed in aggregate as well as by simulation type. Further presentation of spanwise loading distributions and dissection of the results in terms of the impact of individual sub-modelling choices will be presented at the conference and is the subject of a future publication.

A. *Integrated quantities*

The integrated values of rotor power, P, and thrust, T, are compared to the experimental data as coefficients defined as,

$$C_P = \frac{P}{\frac{1}{2}\rho U_\infty^3 \pi D^2/4} \quad \text{and} \quad C_T = \frac{T}{\frac{1}{2}\rho U_\infty^2 \pi D^2/4}, \qquad (2)$$

with ρ the fluid density. The comparison of experimental and blind prediction results is given for both the Low and Elevated (LT) and (ET) turbulence cases in Fig. 3, with the experimental data plotted with a 95% confidence level.

The full set of the L2 submissions shows some banded scatter around the experimental measurements as Fig. 3 illustrates. A quantile-style analysis is adopted to carry out statistical analysis for the submitted C_T and C_P data. The median of the submitted data and a number of quantile ranges were examined, from which we select the 20-80% range to quantify the spread of the submitted L2 data set.

Fig. 3 shows that the median of the L2 submissions exhibits an excellent match to the experimental data, often falling within the latter's uncertainty interval. The Elevated turbulence cases are generally better predicted than those at Low turbulence. The use of the 20-80% spread, shown against the backdrop of all submissions, can be seen as a useful tool to eliminate outliers and quantify the tightness of the banding of the submitted solutions. The 20-80% spread of thrust is relatively tighter than that for power, with less than ±5% across the entire tip-speed ratio range, cf. $+7\% \rightarrow -11\%$ for power.

Fig. 4 presents the power and thrust data for TSRs at, below, and above the optimal TSR for each of the LT and ET cases. Data are presented for both L1 and L2 and the 20-80% spread is presented for all of the data, whilst the actual submission values are presented for the main methodology subsets (due to the small number of data points) to indicate data spread.

Although the median of all the submitted data are close to the measurements across the TSR range, a clear bias can be seen for each category of method. The BEM methods tend to under-predict both the C_T and particularly the C_P for both the LT and ET cases, with a relatively smaller spread in C_T. Additionally, the results using BEM methods show the most spread compared to other techniques, due in part to the diversity of different correction models (e.g. high-induction model, wake correction model, etc) applied. The choice of high thrust induction correction model provides some differences between solutions, with the modified turbulent wake model used by LOMC-BEM yielding very accurate solutions in power, especially for elevated turbulence, over the design and higher TSR range, but curiously over-predicts thrust for these same cases. The Buhl model approach used for high thrust correction by UoE-BEM rendered the most accurate thrust predictions across all TSRs and turbulence levels, but resulted in a consistent under-prediction of power.

BR methods are seen to over-predict thrust and, to a lesser extent, power. The data spread reduces somewhat for the ET case although there are fewer submissions compared to the LT case. Assuming fully turbulent boundary layers, e.g. as when using the SST turbulence model, means that differences between LT and ET blade flows will not be simulated, whilst transitional models may be able to capture earlier blade transition induced by elevated free stream turbulence. At higher TSRs, the blade-local Re is increased and thus differences between BR predictions using fully turbulent and transitional boundary layer models are reduced. Comparison of unsteady and steady MRF based solutions draws no definitive conclusion with differences between mesh resolutions and wall modelling strategies being more important and masking other differences. Solutions that used VOF surface modelling reported limited differences to non-deforming surface modelling approaches for this no-wave case. The CHE-BR-uRANS results were very effective with a significantly lower cell count compared to other methods, whilst returning some of the most accurate solutions.

The AL results are more tightly banded, especially in thrust, than for other methods. However, the sample size is small and some submissions use different sub-models within the same overall model. The biggest differences in C_P for the AL methods arise from the choice of tip-correction model, with those solutions using the Shen et al. correction consistently over-predicting C_P, and those using the modified anisotropic correction of Wimshurst & Willden predicting C_P more accurately. Examination of the blade spanwise loading distributions (not shown) reveals that although not using a tip correction appears to provide accurate integrated results, this masks an over-prediction of loads in the tip region which is balanced by an under-prediction in the mid-span region.

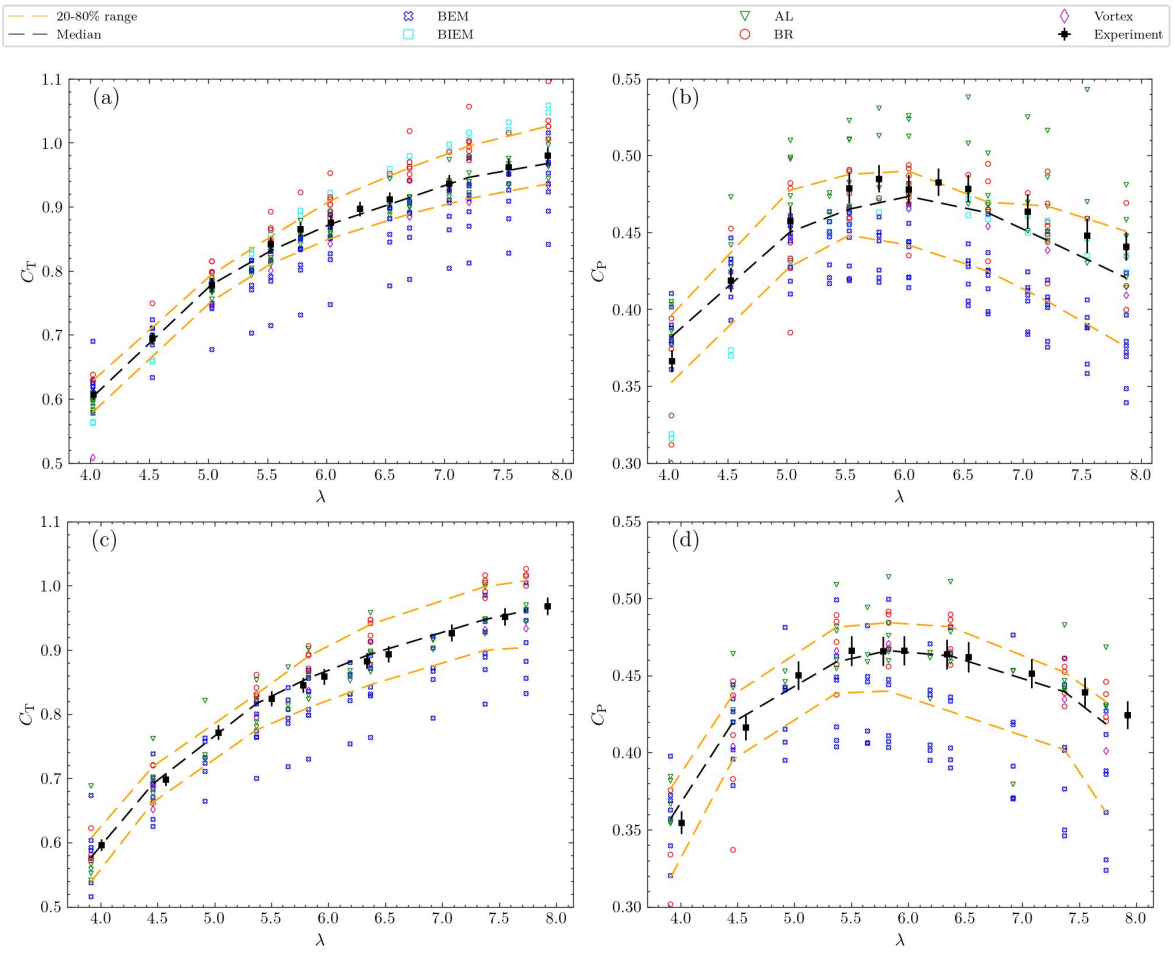

Fig. 3: Thrust and power coefficients, C_T and C_P, for the Low (a-b) and Elevated (c-d) turbulence cases. Experimental data are shown with a 95% confidence level, together with all blind simulation submissions. Submissions are categorised according to modelling techniques, and the median, 50%, and 20-80% data range of all submissions are indicated using dashed lines.

The BIEM results, shown only for LT cases, generally over-predict C_T, especially at high TSR, whereas C_P was under-predicted at low TSR but compared well at high TSR. The solution is found to have some dependency on the numerical parameter used to model the curvature of the wake surface in the tip vortex region, with the D22 submission showing consistently higher C_T and C_P than the D12 submission. The Vortex Method consistently under-predicts both C_T and C_P for LT cases, whilst being more accurate for the ET cases.

Table V presents the normalised standard deviations of C_T and C_P solutions. Standard deviations are computed about the method's median solution value at that TSR, and then normalised on the median value of all data submissions at that TSR (to facilitate comparison between method types). Standard deviations shown in the table are formed by average across the priority TSR cases.

We first consider the change between L1 and L2 submissions. It is clear that correcting user errors reduced the spread of solutions, with the most significant reductions being for AL and BR methods. Conversely, there is only a minor change in BEM solutions reflecting little need for user error correction and perhaps the greater maturity and confidence with which this method is applied; once tip, root, wake correction methods etc are selected, there is limited room for user error.

Once user errors have been corrected, we turn to method comparison based on the L2 data; the standard deviations of the BEM solutions are the largest, reflecting the greater diversity in sub-models available (e.g. root, tip, wake corrections), whilst the AL and BR solutions show the lowest standard deviations for the low and elevated turbulence cases respectively, reflecting the relatively lower degree of modelling choice available within these method categories.

TABLE V: Normalised standard deviations (%) of submitted solutions, C_T and C_P, by method type, ALL, BEM, AL or BR, and submission level, L1 or L2.

Low Turbulence (LT) Cases								
	C_T				C_P			
	All	**BEM**	**AL**	**BR**	**All**	**BEM**	**AL**	**BR**
L1	11.8	6.02	17.1	17.3	15.49	5.15	10.5	15.6
L2	5.45	5.86	2.58	4.80	6.93	4.96	1.64	3.88

Elevated Turbulence (ET) Cases								
	C_T				C_P			
	All	**BEM**	**AL**	**BR**	**All**	**BEM**	**AL**	**BR**
L1	14.7	7.71	2.26	22.8	16.5	6.55	1.54	22.3
L2	6.22	7.44	5.04	3.03	7.87	6.15	4.33	2.56

B. Moment distributions

Simulated time-averaged bending moments are compared to those evaluated by the in-blade sensors in Fig. 5. The bending moments are shown in their non-dimensional form,

$$C_{\mathrm{BM}} = \frac{M}{\frac{1}{2}\rho U_\infty^2 \pi D^3/8}, \tag{3}$$

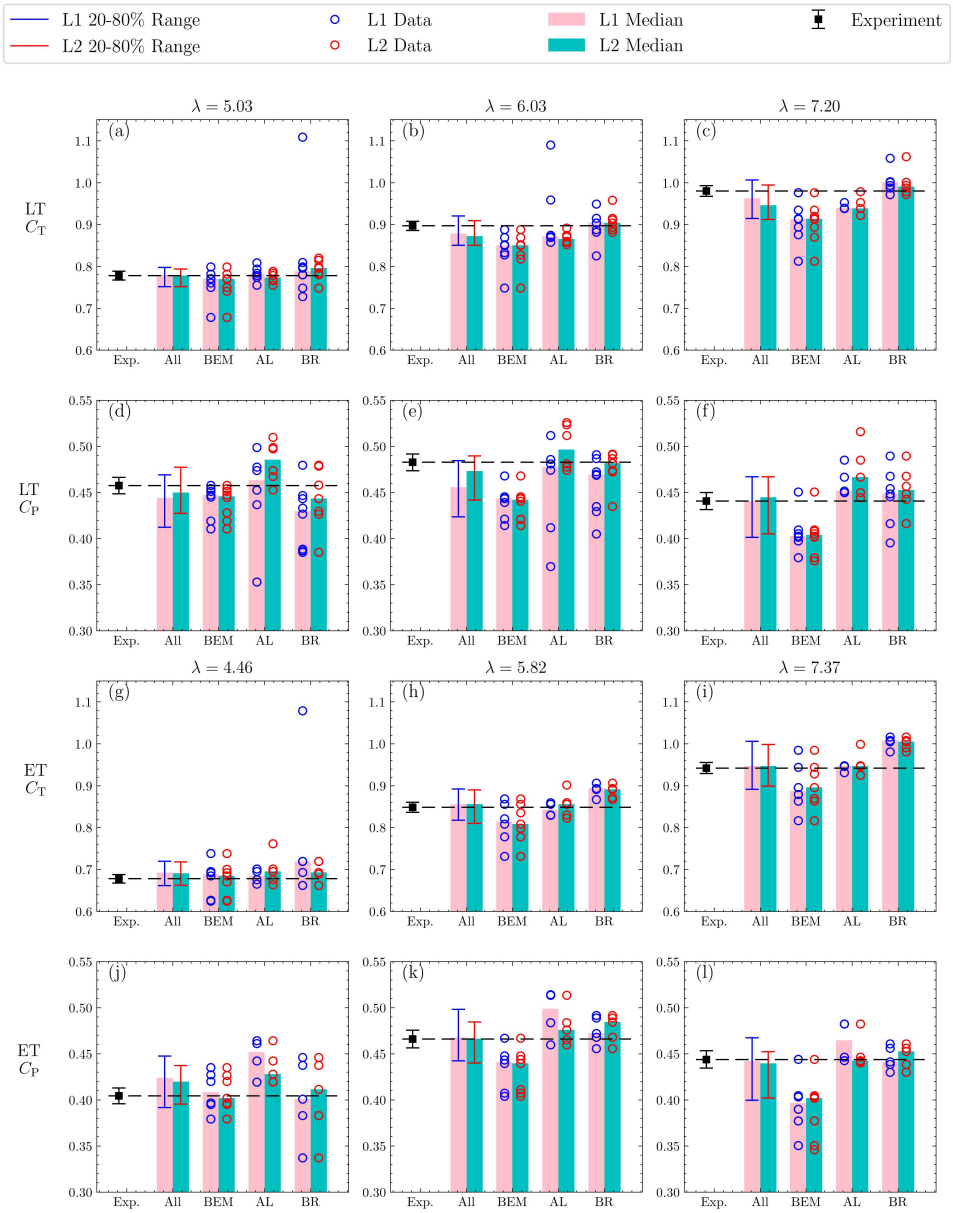

Fig. 4: Medians and ranges of integrated quantities, C_T and C_P, submitted as fully blind (L1) and user-error-corrected (L2) data for Low (LT) and Elevated (ET) turbulence levels. Three tip-speed ratios are shown at, above, and below the design operating point. The vertical bars indicate the 20-80% data range when considering all submissions, whilst the scatter dots are the submission values when considering submission by methodology.

where M denotes the bending moment. Bending moments are accumulative along the blade span and hence very different in magnitude at root and tip, and care must be taken when comparing values across the span and in interpreting the significance of differences between simulations and experiments.

Root bending moments, at $r/R = 0.057$ and denoted C_{RBM}, are shown by median value for each solution type in the flapwise and edgewise directions for the ET case only; see Fig. 6. The standard deviation of the computed C_{RBM} values about the experimental observations (and normalised on the same and then averaged across the priority TSR cases) are presented by method type in Table VI. The figures and table show that the submitted predictions follow closely, with some scatter around, the measurements from the hub position ($r/R = 0.057$) to very close to the blade tip ($r/R = 0.8$).

The BEM solutions generally under-predict the bending moments and have a large spread from the experimental results

TABLE VI: Normalised standard deviation of simulated root bending moments, C_{RBM}, by method type; ALL, BEM, AL or BR, in flapwise and edgewise directions, for LT and ET cases.

	C_{RBM}							
	Flapwise				**Edgewise**			
	All	**BEM**	**AL**	**BR**	**All**	**BEM**	**AL**	**BR**
LT	6.09	7.27	3.84	5.49	17.41	10.89	6.33	8.92
ET	6.45	7.84	4.63	5.58	9.98	10.92	8.37	7.59

comparing to the AL and BR results. This is similar to the observations made in relation to C_T and C_P and is due to the broad variety of BEM sub-models used.

The AL solutions have a constant small over-prediction of the bending moments, especially in the edgewise direction, which is consistent with the general small over-prediction in C_P. Most of the over-predicted AL solutions are from simulations in which either tip-loss models haven't be used

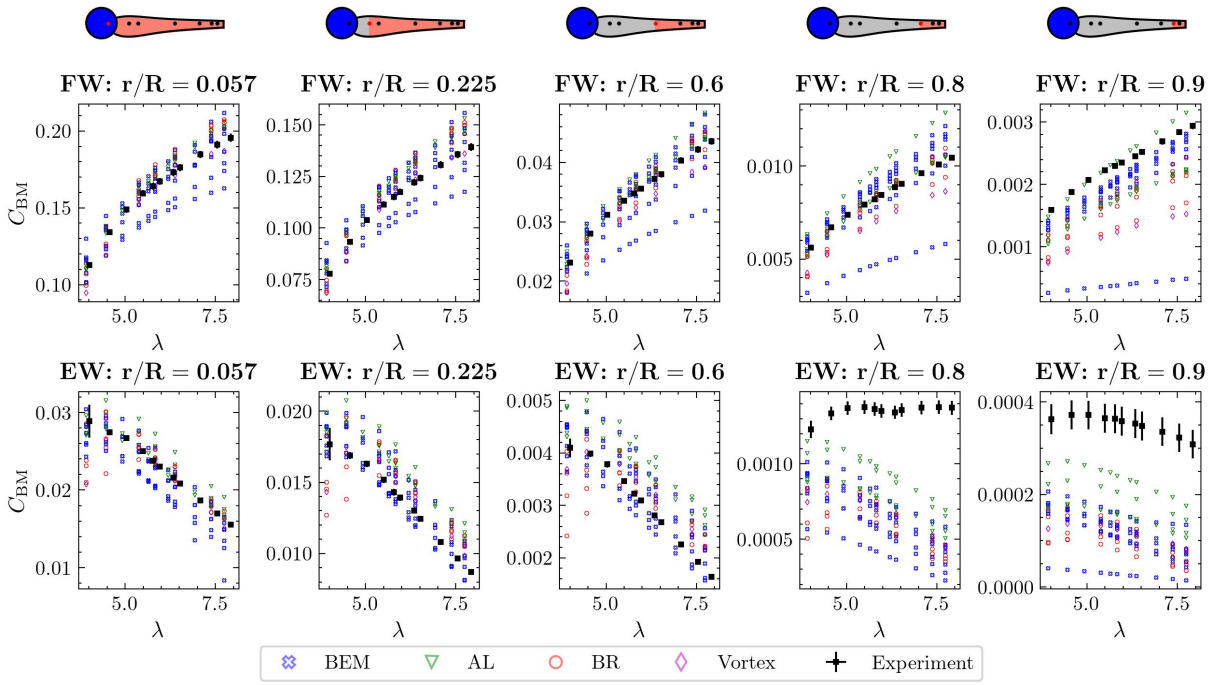

Fig. 5: Bending moment coefficients, C_{BM}, across the tip-speed ratio sweep for the different simulation techniques with comparison to experiments. Elevated turbulence case only. Flapwise (FW) and edgewise (EW) bending moments are presented in the top and bottom rows respectively, with the blade diagrams at the top of the figure indicating the locations of the sensors and the shaded portions representing the regions of the blade contributing to the bending moments at each of the measurement locations. Note the very different ranges of C_{BM} in sub-plots between blade tip and root.

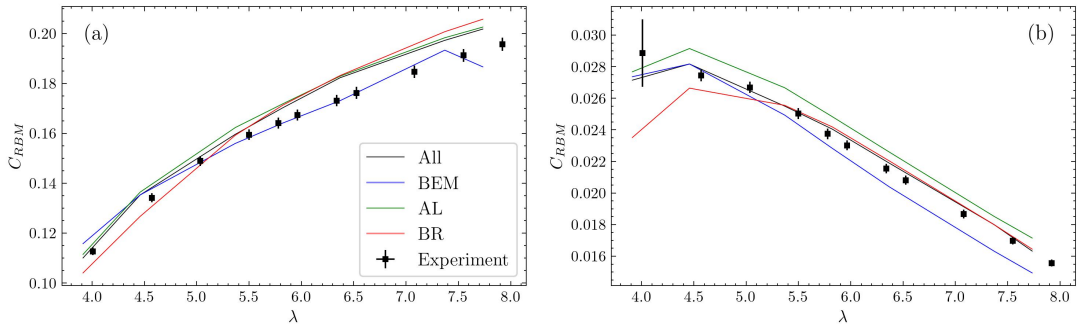

Fig. 6: Root bending moment coefficients, C_{RBM}, in flapwise (a) and edgewise (b) directions plotted by simulation method (median values) together with experiments for the elevated turbulence case.

or less aggressive isotropic Shen-type models have been used.

The BR results lie further away from the measured bending moments in the low TSR range, likely owing to the hydrofoil being close to the early stall region and the difficulties of simulating this. Whilst for $\lambda \geq 5.0$, the BR submissions give very encouraging predictions of bending moments and provide the most accurate predictions in the edgewise direction.

Although there are significant differences between the submissions and experimental bending moments in the tip region, the bending moments here are very small, and consequently these differences have little impact on the accuracy of root bending moment predictions. The simulated bending moments near the tip ($r/R \geq 0.8$) have similar trends with increasing TSR, and particularly in the edgewise direction depart from the experimental trend. We note that for both the flapwise and edgewise bending moments to be under-predicted in the tip region requires a drop in the blade lift force which could be caused by a reduction in the local angle-of-attack. Whilst the rotor blades were simulated as rigid, they do of course deflect and twist experimentally. We postulate that the experimental blades twisted in the tip region so as to increase the local of angle-of-attack, leading to the out-of-trend variation in the outboard edgewise bending moment with TSR, and the divergence between simulated and experimental data over the outboard section of the blade $r/R \geq 0.8$. Uncoupled Finite Element Analysis of the blade's deformation under the simulated loading distribution confirms the direction and magnitude of the implied angle-of-attack change in this region.

V. Conclusions

Blind comparisons between model predictions and experimental test results were extremely positive, with median power and thrust in close agreement with experiments. Whilst individual solutions using BEM, BR, AL, BIEM or Vortex methods were found to be accurate for given cases, there was a general tendency for BEM and Vortex methods to under-predict integrated power and thrust, whilst BR methods tend

to minorly over-predict as do AL methods, with BIEM showing over-prediction in thrust. In the case of BEM and AL methods the choice of sub-models (high-induction, tip-loss correction etc) can have a significant impact on accuracy.

In-blade bending moment measurements enabled blind predictions of spanwise load variation. Although there is some scatter around measurements, there are also clear biases dependent on solution method which correlate well with biases in prediction of power and thrust. Flapwise and edgewise bending moments are encouragingly well predicted across blade mid-spans, and root bending moment predictions are particularly robust. Out-board loading is consistently under-predicted, particularly edgewise, but this is believed to be due to twist deformation of the blades during the experiment.

The benchmarking exercise has demonstrated that the large model-scale experimental turbine data provides a robust data set against which researchers and design engineers can test their models and implementations to ensure robustness in their processes, helping to reduce uncertainty and provide increased confidence in engineering processes.

Acknowledgement

The benchmarking exercise was jointly funded by the Supergen ORE Hub, grant number EP/S000747/1, and by RHJW's EPSRC Advanced Fellowship, EP/R007322/1.

This work was authored in part by the National Renewable Energy Laboratory, operated by Alliance for Sustainable Energy, LLC, for the U.S. Department of Energy (DOE) under Contract No. DE-AC36-08GO28308. Funding provided by U.S. Department of Energy Office of Energy Efficiency and Renewable Energy Water Power Technologies Office. The views expressed in the article do not necessarily represent the views of the DOE or the U.S. Government. The U.S. Government retains and the publisher, by accepting the article for publication, acknowledges that the U.S. Government retains a nonexclusive, paid-up, irrevocable, worldwide license to publish or reproduce the published form of this work, or allow others to do so, for U.S. Government purposes.

References

[1] A. Bahaj, W. Batten, and G. McCann, "Experimental verifications of numerical predictions for the hydrodynamic performance of horizontal axis marine current turbines," *Renewable Energy*, vol. 32, no. 15, 2007.

[2] B. Gaurier, G. Germain, J. Facq, C. Johnstone, A. Grant, A. Day, E. Nixon, F. Di Felice, and M. Costanzo, "Tidal energy "Round Robin" tests comparisons between towing tank and circulating tank results," *Int. J. Marine Energy*, vol. 12, pp. 87–109, 2015.

[3] G. S. Payne, T. Stallard, and R. Martinez, "Design and manufacture of a bed supported tidal turbine model for blade and shaft load measurement in turbulent flow and waves," *Renewable Energy*, vol. 107, 2017.

[4] B. Gaurier, M. Ikhennicheu, G. Germain, and P. Druault, "Experimental study of bathymetry generated turbulence on tidal turbine behaviour," *Renewable Energy*, vol. 156, pp. 1158–1170, 2020.

[5] L. Luznik, K. A. Flack, E. E. Lust, and K. Taylor, "The effect of surface waves on the performance characteristics of a model tidal turbine," *Renewable Energy*, vol. 58, pp. 108–114, 2013.

[6] J. McNaughton, B. Cao, A. Nambiar, T. Davey, C. R. Vogel, and R. H. Willden, "Constructive interference effects for tidal turbine arrays," *J. Fluid Mechanics*, vol. 943, p. A38, 2022.

[7] R. Willden, S. Tucker Harvey, X. Chen *et al.*, "Unsteady loading tidal turbine benchmarking study." [Online]. Available: https://supergen-ore.net/projects/tidal-turbine-benchmarking

[8] S. Tucker Harvey *et al.*, "Tidal turbine benchmarking project: Stage I - steady flow experiments," in *Proc. 15th EWTEC*, 2023.

[9] H. Cerón-M, F. Catalano, and A. C. Filho, "Experimental study of the influence of vortex generators on airfoils for wind turbines," in *VI Congreso Internacional de Ingeniería Mecánica*, 2013.

[10] C. Bak, P. Fuglsang, J. Johansen, and I. Antoniou, "Wind tunnel tests of the NACA 63-415 and a modified NACA 63-415 airfoil," in *RISØ-R–1193*, 2000.

[11] S. A. Ning, "A simple solution method for the blade element momentum equations with guaranteed convergence," *Wind Energy*, vol. 17, no. 9, pp. 1327–1345, 2014.

[12] F. Zilic de Arcos, "Hydrodynamics of highly-loaded axial flow tidal rotors," Ph.D. dissertation, University of Oxford, 2021.

[13] National Renewable Energy Laboratory, "AeroDyn users guide and theory manual." [Online]. Available: https://openfast.readthedocs.io/en/main/source/user/aerodyn/index.html

[14] I. Masters, J. Chapman, M. Willis, and J. Orme, "A robust blade element momentum theory model for tidal stream turbines including tip and hub loss corrections," *J. Marine Eng. & Tech.*, vol. 10, pp. 25–35, 2011.

[15] M. Togneri, G. Pinon, C. Carlier, C. Choma Bex, and I. Masters, "Comparison of synthetic turbulence approaches for blade element momentum theory prediction of tidal turbine performance and loads," *Renewable Energy*, vol. 145, pp. 408–418, 2020.

[16] G. T. Scarlett and I. M. Viola, "Unsteady hydrodynamics of tidal turbine blades," *Renewable Energy*, vol. 146, pp. 843–855, 2020.

[17] M. Drela, "XFOIL: An Analysis and Design System for Low Reynolds Number Airfoils," in *Low Reynolds Number Aerodynamics*. Springer, Berlin, Heidelberg, 1989, pp. 1–12.

[18] D. Marten, J. Wendler, G. Pechlivanoglou, C. N. Nayeri, and C. O. Paschereit, "QBLADE: an open source tool for design and simulation of horizontal and vertical axis wind turbines," *Int. J. Emerging Technology & Advanced Engineering*, vol. 3, no. 3, 2013.

[19] D. A. Spera, "Models of lift and drag coefficients of stalled and unstalled airfoils in wind turbines and wind tunnels," Tech. Rep., 2008.

[20] Z. Du and M. Selig, "A 3D stall-delay model for horizontal axis wind turbine performance prediction," in *ASME Wind Energy Symp.*, 1998.

[21] D. Apsley and P. Stansby, "Unsteady thrust on an oscillating wind turbine: Comparison of blade-element momentum theory with actuator-line CFD," *J. Fluids & Structures*, vol. 98, p. 103141, 2020.

[22] H. Mullings and T. Stallard, "Analysis of tidal turbine blade loading due to blade scale flow," *J. Fluids & Structures*, vol. 114, p. 103698, 2022.

[23] P. Ouro, H. Mullings, and T. Stallard, "Establishing confidence in predictions of fatigue loading for floating tidal turbines based on large-eddy simulations and unsteady blade element momentum," in *5th Int. Conference on Renewable Energies Offshore*, 2023, pp. 915–924.

[24] J. N. Sorensen and W. Z. Shen, "Numerical modeling of wind turbine wakes," *J. Fluids Eng.*, vol. 124, no. 2, pp. 393–399, 2002.

[25] P. Schmitt and D. Robinson, "A coupled actuator line and finite element analysis tool," *OpenFOAM Journal*, vol. 2, p. 81–93, 2022.

[26] P. Bachant, A. Goude, and M. Wosnik, "Actuator line modeling of vertical-axis turbines," 2018.

[27] W. Z. Shen, R. Mikkelsen, J. N. Sørensen, and C. Bak, "Tip loss corrections for wind turbine computations," *Wind Energy*, vol. 8, no. 4, pp. 457–475, 2005.

[28] P. Ouro, P. K. Stansby, and T. Stallard, "Analysis of the kinetic energy recovery behind a tidal stream turbine for various submergence levels," *International Marine Energy Journal*, vol. 5, no. 3, pp. 265–272, 2022.

[29] J. Schluntz and R. H. Willden, "An actuator line method with novel blade flow field coupling based on potential flow equivalence," *Wind Energy*, vol. 18, no. 8, pp. 1469–1485, 2015.

[30] A. Wimshurst and R. Willden, "Analysis of a tip correction factor for horizontal axis turbines," *Wind Energy*, vol. 20, no. 9, 2017.

[31] M. Zormpa, F. Z. de Arcos, X. Chen, C. Vogel, and R. Willden, "Sensitivity of wind turbine aerodynamics to actuator line model parameters," in *Wind Energy Science Conference 2023*, 2023.

[32] G. Vaz, F. Jaouen, and M. Hoekstra, "Free-Surface Viscous Flow Computations: Validation of URANS Code FreSCo," ser. Int. Conf. OMAE, vol. 5: CFD and VIV, 2009, pp. 425–437.

[33] W. Otto, D. Rijpkema, and G. Vaz, "Viscous-Flow Calculations on an Axial Marine Current Turbine," ser. Int. Conf. OMAE, vol. 7: Ocean Renewable Energy, 2012, pp. 369–382.

[34] D. Calcagni, F. Salvatore, and R. Muscari, "CFD analysis of a horizontal-axis turbine in the framework of a blind-test tidal benchmarking project," in *Proc. of the 33rd Int. Ocean and Polar*, 2023.

[35] M. de Oliveira, R. C. Puraca, and B. S. Carmo, "Assessment of turbulence models for the simulation of the flow through a megawatt scale wind turbine rotor," in *ABCM (Ed.), EPTT-2022*, 2022.

[36] ——, "Blade-resolved numerical simulations of the NREL offshore 5 MW baseline wind turbine in full scale: A study of solver configuration and discretization strategies," *Energy*, vol. 254, p. 124368, 2022.

[37] F. Salvatore, Z. Sarichloo, and D. Calcagni, "Marine turbine hydrodynamics by a boundary element method with viscous flow correction," *J. Marine Science & Engineering*, vol. 6, no. 2, p. 53, 2018.

[38] G. Pinon, P. Mycek, G. Germain, and E. Rivoalen, "Numerical simulation of the wake of marine current turbines with a particle method," *Renewable Energy*, vol. 46, pp. 111 – 126, 2012.

[39] C. Choma Bex, M.-A. Dufour, Y. Ben Belkacem, G. Pinon, G. Germain, and E. Rivoalen, "Tidal and wind turbine simulation with the simulation code DOROTHY," in *Proc. RENEW*, 2022, pp. 113–122.